OPTIMIZATION OF SAIL DESIGN

by

Thomas John Dunyak

Thesis submitted to the Faculty of the
Virginia Polytechnic Institute and State University
in partial fulfillment of the requirements for the degree of
MASTER OF SCIENCE
in
Engineering Mechanics

APPROVED:

Dean T. Mook

Manohar P. Kamat

Ali H. Nayfeh

June, 1983
Blacksburg, Virginia

TABLE OF CONTENTS

LIST OF FIGURES

Chapter I

INTRODUCTION

In the past, sail design was primarily a trial-and-error technique. A master sail designer would slightly modify a working sail plan. If the modification improved the overall effectiveness of the sail, he would again attempt some slight modification. However, if the change was ineffective, the designer would regress to the prior sail plan and try something new. In spite of this slow and cumbersome technique, present sail designs are fairly effective.

There is still considerable room for improvement, though, and over the past ten years computers have started to play a small role in sailboat design. Although many hull designs are now based on computer techniques, computers have had a very limited impact on sail designs. There are several reasons for this lack of development. The sail is a very complicated lifting surface. It has large camber and twist. (In other words, the curvature near the top of the sail is different than curvature at the bottom.) Also, the sail's triangular shape and the interaction between sails complicate the analysis. Finally, the sail works in the earth's boundary layer, and this boundary layer is very complex. However, with the recent developments in finite elements, this sail problem is beginning to recieve more attention.

The first computer application to sail design was a two-dimensional analysis of the flow across the sail (Milgram, 1972). Then, a three-dimensional analysis had been attempted by Thrasher, Mook, and Nayfeh (1979). This attempt proved very successful. Therefore, the next step is to optmize the sail. In our research, we could not find any published attempts to optimize sail design through the use of computers. As a result, the program developed in this project could set the state of the art in computer-based sail design.

There are four major areas to consider when developing this type of program: modeling the sail, analyzing the model, developing an optimization technique, and applying this technique to the model. The first couple sections of this report describe the model of the sail and the analysis of this model. The next section presents the optimization of the unconstrained problem. The final sections add the effects of a separation constraint and present the final results for the constrained problem.

Chapter II

THE VARIABLES AND THEIR RELATIONSHIP TO THE MODEL

As air flows past a sail, the air on top in figure 1 flows faster than the air on the bottom. Therefore, a pressure differential results, and consequently, there will be a force on the sail. This resultant force can be broken into two components, a heeling force which leans the boat over and a driving force which propels the boat through the water. This driving force is the dependent variable that will be optimized. In order to analyze the sail, a chordwise arc is approximated by a series of short straight lines called chords. The orientation of each chord is specified by an angle labelled θ_i in figure 2. The length of each chord is held constant. Therefore, the angles θ_i in figure 2 will be the independent variables.

To produce the optimum sail, each angle θ_i will be systematically varied until a set of angles $(\theta_1,\theta_2,\ldots,\theta_n)$ that produces an optimum driving force is found. Once these angles have been determined, the optimum lattice points in the sail can eacily be calculated. From this information, the sailmaker could cut the optimum sail.

Chapter III

ANALYSIS OF THE MODEL

In order to analyze the sail, we idealize the sail cloth as an infinitely thin vortex sheet. Figure 3 shows these ideas associated with a vortex sheet. Next the distributed vorticity is represented by concentrated cores of vorticity at distinct points, called vortex points. The cores have finite circulations around them. In order to represent the sail cloth, a no-penetration boundary condition should be imposed along the entire model but is only imposed at the control points C. Also, according to the Kutta condition, the vorticity at the trailing edge is equal to zero.

On the sail model, a point vortex is located at one-quarter the length of each chord, and a control point is located at three-quarters the length of each chord. Figure 4 shows a two-dimensional model of a sail with four elements. The control points are labeled C_i. The vortex points are labeled V_i, and the circulations are labeled Γ_i.

The locations of these control points and vortex points are not totally arbitrary. First, consider a flat plate of length L in a uniform stream at a specified angle of attack. Upon analyzing the plate, we determine a lifting force and a resulting moment about the center of the plate. Now model

the plate with a vortex point at one-quarter L and a control point at three-quarters L. By varying the magnitude of the circulation at the vortex point so as to impose a no-penetration condition at the control point, we produce a set of forces that is statically equivalent to that in the above solution. The sail is represented as a series of flat plates at different angles of attack.

Next, the circulation at each vortex point must be calculated. Using the Biot-Savart law (see Appendix A), we determine the effect of the circulations at each control point. Although this analysis can be applied to any number of elements, a four-element model is described for the sake of simplicity. The effect of the circulations on the first control point is

$$h_{11}\Gamma_1 + h_{12}\Gamma_2 + h_{13}\Gamma_3 + h_{14}\Gamma_4 = -V^1_{fsn}$$

where V^i_{fsn} is the normal component of the wind velocity at the first control point and h_{1i} is the effect of the ith circulation on the first control point normal to the vortex sheet. Similarily, the effect on the other control points can be calculated. As a result, the following set of equations is produced:

$$h_{11}\Gamma_1 + h_{12}\Gamma_2 + h_{13}\Gamma_3 + h_{14}\Gamma_4 = -V^1_{fsn}$$

$$h_{21}\Gamma_1 + h_{22}\Gamma_2 + h_{23}\Gamma_3 + h_{24}\Gamma_4 = -V^2_{fsn}$$

$$h_{31}\Gamma_1 + h_{32}\Gamma_2 + h_{33}\Gamma_3 + h_{34}\Gamma_4 = -V^3_{fsn}$$

$$h_{41}\Gamma_1 + h_{42}\Gamma_2 + h_{43}\Gamma_3 + h_{44}\Gamma_4 = -V_{fsn}$$

In matrix form, these equations become

$$[h]\ \{\Gamma\} = -\{V_{fsn}\}$$

Next, a Gauss-Seidel iterative technique is used to calculate the values of Γ_i.

After determining the circulations, we calculate the pressure distribution on the sail. To assist the understanding of the calculations, refer to the typical element in figure 5. A surface of length L is drawn through a vortex point and a control point. This surface represents an element of the sail. Next, the velocities are represented on the surface. In figure 6, the velocities on the ends of the elements (V_e) are equal to zero by the no-penetration constraint. In order to relate the tangential velocities to the circulations, we consider Stoke's theorem:

$$\oint_C \bar{A} \cdot d\bar{r} = \int_S \int \text{curl } \bar{A} \cdot \bar{N}\, ds$$

We then apply Stoke's theorem to the surface of the element.

$$\oint_C \bar{V} \cdot d\bar{r} = V_{tL} - V_{bL} = \iint \text{curl } \bar{V} \cdot \bar{N}\, ds$$

$$V_{tL} - V_{bL} = \Omega t L = \Gamma$$

where Ω is the vorticity and t is the thickness of the element. Therefore,

$$V_t - V_b = \frac{\Gamma}{L} = \Delta V$$

Applying this equation to figure 6 results in the equation

$$\Delta V_i = \frac{\Gamma_i}{L}$$

where L is the length of the element and ΔV_i is the jump in the tangential component of the velocity at the control point of element i.

We now use Bernoulli's equation to determine the pressures. Bernoulli's equation is

$$\frac{P_c}{\rho} + \frac{1}{2} V_c^2 = \frac{P_\infty}{\rho} + \frac{1}{2} V_\infty^2$$

where P_c is the pressure at the control point, V_c is the velocity at the control point, ρ is the density of the air, P_∞ is the free-stream pressure, and V_∞ is the freestream velocity. Rearranging this equation produces the result

$$\frac{P_c - P_\infty}{\frac{1}{2} \rho V_\infty^2} = 1 - \frac{V_c^2}{V_\infty^2}$$

We define the pressure coefficient as

$$Cp_c = \frac{P_c - P_\infty}{\frac{1}{2} \rho V_\infty^2}$$

Therefore, the following equations are used to calculate the pressure coefficients

$$Cp = 1 - V^2$$

and

$$Cp_t = 1 - V_t^2$$

$$Cp_b = 1 - V_b^2$$

where the subscript t refers to the top of the sail, and b refers to the bottom of the sail. Also, each of these velocities are normalized with respect to the freestream velocity. Now, equations for V_t and V_b are developed.

$$V_t = \tilde{V} + \frac{1}{2}\Delta V$$

and

$$V_b = \tilde{V} - \frac{1}{2}\Delta V$$

where V is the magnitude of the sum of the freestream velocity and the velocities calculated from the vorticities. Therefore,

$$Cp_t = 1 - \tilde{V}^2 - \tilde{V}\Delta V - \frac{1}{4}\Delta V^2$$

$$Cp_b = 1 - \tilde{V}^2 + \tilde{V}\Delta V - \frac{1}{4}\Delta V^2$$

$$\Delta Cp = 2\tilde{V}\Delta V$$

where ΔCp is the pressure jump across the sail at the control point.

In addition to the control points, pressure coefficients are calculated upstream of the leading edge and downstream of the trailing edge. These lengths are termed ΔL_{le} and ΔL_{te} respectively, and figure 7 shows ΔL_{le} and ΔL_{te} on a four element model. Since both of these points are removed from the vortex sheet, ΔV is identically zero. Therefore,

$$Cp_{le} = 1 - \tilde{V}^2_{le}$$

$$Cp_{te} = 1 - \tilde{V}^2_{te}$$

Unfortunately, ΔL_{le} and ΔL_{te} have a major effect on the optimum drive. These effects will be investigated in a later section.

The last step in the analysis involves the calculation of the drive. From potential flow theory, we know that a circulation superimposed in a uniform stream produces a lift (L). Such that

$$L=\rho U_\infty \Gamma$$

where Γ is the magnitude of the circulation and L is normal to the free-stream velocity. In our case, we have N circulations. Therefore,

$$L=\rho U_{\infty} \sum_{i=1}^{n} \Gamma_i$$

Since the drive is the x-component of the lift, we can say

$$\text{Drive}=L \bullet \text{UNX}$$

where

$$\text{UNX}=\sin(\text{attack angle})$$

or

$$\text{Drive}=\rho U_{\infty}(\text{UNX}) \sum_{i=1}^{n} \Gamma_i$$

Now by defining

$$\text{CIRC}= \sum_{i=1}^{n} \Gamma_i$$

we have

$$\text{Drive}=\rho U_{\infty}(\text{CIRC})\text{UNX}$$

However, ρ, U_{∞} and UNX are all constants. Therefore, by maximizing CIRC, we maximize the drive. As a result, the problem reduces to an optimization of CIRC.

Overall, the analysis of the flow involves five steps. First, the sail is represented by a vortex sheet and then approximated by discrete vortex points. Next, the Biot-Savart law is applied to determine the velocity field generated by the discrete vorticity subject to the the no penetration constraint. Then, the velocity differences are calculated, and finally, these velocities are used to calculate the pressure coefficients and CIRC.

In order to test this part of the program, a circular arc and a flat plate were analyzed. In the case of a flat plate, the numerically obtained circulation closely matched the analytical results. For the circular arc, the numerically obtained values were slightly smaller than the analytical values. However, as more elements were used to approximate the arc, our solution converged to the analytic solution. Therefore, the program will analyze the sail with sufficient accuracy. Located in figure 8 is a table showing this convergence for the circular arc.

Chapter IV

OPTIMIZATION OF THE UNCONSTRAINED PROBLEM

In order to optimize the unconstrained problem, we first calculate the gradient of CIRC and then use this gradient in an optimization algorithm. The existing computer code incorporates a center-difference method to calculate the gradient. Overall, three different algorithms are used to optimize CIRC. The first method is termed the gradient method. Once an initial guess is made and the gradient is calculated, we march along this gradient direction until an optimum is reached. At this point, a new gradient is calculated, and a new optimum is found. The method continues in this manner until the global optimum is reached. As can be imagined, this method is very inefficient and cumbersome.

The second method for optimization is a typical conjugate gradient method (Fletcher, 1964). However, since we are dealing with a very nonlinear problem, this method is also inefficient. The third method incorporates a routine developed by Argonne Labratories and is based on Powell's method. This routine is called VMCON. Although this routine is primarily used for constrained optimization, it proves very effective for this application. Located in Appendix C is a brief synopsis of VMCON as applied to the constrained problem.

Figures 9 and 10 present results for a six-element model and a twelve-element model. These results are obtained regardless of the initial conditions and the optimization scheme used in the analysis. In this section, we are merely considering optimization of the unconstrained problem. In the subsequent section, we introduce a separation constraint into the problem and then determine the effects of this constraint. As can be expected, these effects are are very pronounced.

Chapter V

THE SEPARATION CONSRTAINT AND ITS EFFECTS

In the preceeding section, we discussed a theoretical optimum sail. However, the actual optimum sail may be much different. This is due to a phenomenon called separation. In order to perform at maximum effectiveness, the sail must have a smooth flow along its surface (figure 11). However, if the curvature of the sail is too large, the flow may separate from the sail, and a turbulent wake will develop (figure 12). This wake on the backside of the sail will greatly reduce the overall performance of the sail. For example, for a sail defined by only two angles θ_1 and θ_2, an ideal flow may produce force contours similar to those in figure 13. Theoretically, the optimum driving force occurs at point A. However, separation occurs for any point to the right of the dashed line, and actually the optimum driving force occurs at point B. Therefore, point B is the desired set of conditions to maximize the driving force.

To incorporate this separation constraint into the problem, we use an integrated version of Stratford's separation criterion (1959). Statford's citerion states that separation will occur if the following inequality is satisfied:

$$.39(10^{-6}\ Re)^{\frac{1}{10}} - Cp(s\ \frac{dCp}{ds})^{\frac{1}{2}} \leq 0$$

where

$$Re = \frac{U_\infty L}{\nu}$$

U_∞ is the freestream velocity, L is the chord length and ν is the kinematic viscosity. Integrating this equation, we get

$$[.39(10^{-6}\ Re)^{\frac{1}{10}}]^2 \ln\left(\frac{s}{s_0}\right) - \frac{1}{3} Cp^3 + \frac{1}{3} Cp_0^3 \leq 0$$

where s_0 and Cp_0 correspond to the first point where

$$\frac{dCp}{ds} \geq 0$$

In the optimization routine, we fit a cubic spline through the values of Cp at the control points. Located in Appendix B is a description of this cubic interpolation. Next, we set

$$SEP = [.39(10^6\ Re)^{\frac{1}{10}}]^2 \ln\left(\frac{s}{s_0}\right) - \frac{1}{3} Cp^3 + \frac{1}{3} Cp_0^3$$

and evaluate SEP along the entire length of the sail. Therefore, for separation not to occur,

$$\text{minimum}(SEP) \geq 0$$

As a result, the following constrained optimization problem is produced:

maximize (CIRC)

subject to

minimum(SEP)≥0

In this case, The problem is rewritten as

minimize (-CIRC)

subject to

minimum(SEP)≥0

We can now apply the VMCON optimization algorithm to the second form of the constrained problem. Located in Appendix C is a description of VMCON as applied to the unconstrained problem.

Chapter VI

RESULTS FROM THE CONSTRAINED PROBLEM

After completing the analysis we now run several cases to test the the validity of this analysis. The majority of the cases involve a six-element model. Located in each figure is a plot of the optimum shape corresponding to the inputed parameters, the angles associated with this plot, and the optimum value of CIRC.

Figure 14 presents the results for a six-element model at a 60° angle of attack. In this case, we let ΔL_{le}=.125 and ΔL_{te}=0.0. In the next series of cases, we will test the effects of various values of ΔL_{le} and ΔL_{te}. Located in figures 15, 16, and 17 are plots of pressure disturbutions over the sail. Figure 15 shows the disturbution over the top of the sail, and figure 16 shows the disturbution over the bottom of the sail. The last plot, figure 17, indicates the pressure difference across the sail. In our analysis, we found the model predicts separation is impending at the trailing edge. However, figure 17 indicates that this portion of the sail has only a small contribution to the total drive. Therefore, the small error in Stratford's criterion is considered negligible on the optimum drive.

As stated above, the location of ΔL_{le} and ΔL_{te} have a significant effect on the shape of the sail and subsequently the drive. Figure 18 plots values of Circ versus ΔL_{te}, and figure 19 shows the relationship between Circ and ΔL_{te}. In all of these runs we considered a six-element model at 60° angle of attack. Unfortunately, without reliable wind tunnel data, we cannot make an exact choice of ΔL_{le} and ΔL_{te}. As a result, we set ΔL_{le}=.125 and ΔL_{te}=0.0 in all of the following cases.

Figure 20 compares a six element model and a twelve element at a 60° attack angle. Note the similarity between the two results. Although more elements slightly improve the sail representation, this advantage is offset by drastic increase in computer time. Therefore, we feel the six element model accurately represents the sail.

Located in figures 21, 22, 23, and 24 are results from various angles of attack. Note that higher angles of attack have a flatter sail or less camber. Unfortunately, at angles of attack higher than 90°, the sail becomes less and less a lifting surface. As a result, for these very high angles of attack, this analysis does not apply.

Chapter VII

FUTURE WORK

Although the project has produced very satisfying results, the three-dimensional problem must now be tackled. Fortunately, the three-dimensional analysis is a direct extension of the two-dimenional problem. For examples, the vortex-lattice analysis is basically the same, and once the pressure coefficients have been determined, the two-dimensional Stratford's separation criterion can be applied. In addition, although the number of independent variables will increase, the application of VMCON is exactly the same in both analyses. Therefore, although the two-dimensional analysis has little impact on actual sail design, it is a significant and necessary step towards a major development in computer-aided sail design.

There are several benifits associated with a three-dimensional analysis. Most sailboats have two sails, a mainsail and a jibsail. A three-dimensional analysis can easily incorporate interactive effects between these sails. This analysis can then be extended to include any number of interacting sails. Also, the rake of the mast can be entered into the problem as a independent variable. Similarly, the length of the roach can be optimized subject to structural

constraints. Since a sail works in the earth's boundary layer, these effects can also be considered. Overall, the three-dimensional case poses a very challenging problem. As of April 1983, a significant amount of work has already been devoted to this three-dimensional problem, and the work is continuing. In the next couple months, we hope to finish a major portion of this problem and soon after present these results.

Appendix A

THE BIOT-SAVART LAW

One of the most important tools used in the analysis is the Biot-Savart law. Therefore, the law itself is more fully explained in this section. Basically the law determines the effect of a disturbance at some removed point. This law is a fundamental building block for any field theory, and it can be applied to magnetic fields, flow fields or any number of other applications. In this project, we incorporated the Biot-Savart Law to calculate the influence of a circulation at a control point.

In figure 25, the points A and B define a vortex element. The velocity field is irrotational. The circulation around the vector $\overline{AB}$ has magnitude Γ. Point C is the position were the velocity is desired. $\overline{R}_1$ is the vector going from point A to point C, and θ_1 is the angle between $\overline{R}_1$ and $\overline{AB}$. $\overline{R}_2$ is the vector from point B to point C, and θ_2 is the angle between $\overline{R}_2$ and $\overline{AB}$. H is the perpendicular distance from point C to the vector $\overline{AB}$, and $\overline{EV}$ is a unit vector orthogonal to $\overline{R}_1$ and $\overline{R}_2$. Therefore, $\overline{EV}$ is also orthogonal to AB. According to the Biot-Savart law

$$\overline{V} = \frac{\Gamma}{4\pi h}(\cos\theta_1 - \cos\theta_2)\overline{EV}$$

where

$$\overline{EV} = \frac{\bar{R}_1 \times \bar{R}_2}{|\bar{R}_1| \; |\bar{R}_2|}$$

and $\bar{V}$ is the velocity at C. Figure 26 shows the magnitude of the velocity as a function of the perpendicular distance from the vortex element. In this figure, Γ, θ_1 and θ_2 are constant. Note that as the point is moved away from the vortex element the effect of the circulation decreases.

Appendix B

THE CUBIC SPLINE

In order to locate the separation point from Stratford's equation an interpolation polynomial must be used. This appendix describes the development of a cubic interpolation polynomial. We let F(s) be a function that is to be interpolated. F(s) is known only at the points s_1 through s_n. S(s) is the function that approximates F(s). S(s) is a piecewise function such that

$$S(s)=S_j(s)$$

when

$$s_j \leq s \leq s_{j+1}$$

for j=1,2,...,n. Also, S_j is a cubic polynomial in s. We let

$$h_j = s_{j+1} - s_j$$

and

$$F_j = F(s_j)$$

Then

$$S_j''(s) = \frac{Y_j}{h_j}(s_{j+1}-s) - \frac{Y_{j-1}}{h_j}(s-s_j)$$

where the set of Y_j are the values (unknown at this point) of the second derivatives of S at the points where F(s) is known.

Integrating equation (1) twice leads to the equation

$$S_j(s) = \frac{Y_j}{6h_j}(s_{j+1} - s)^3 + \frac{Y_{j+1}}{6h_j}(s - s_j)^3 + C_j(s - s_j) + D_j(s_{j+1} - s) \tag{2}$$

We note that equation (2) contains two constants of integration, C_j and D_j. Also, the last two terms of equation (2) are linear functions of s in terms of these two constants. To make S(s) continuous and interpolate F(s), we must choose C_j and D_j such that

$$S_j(s_j) = F_j = \frac{1}{6} Y_j h_j^2 + D_j h_j \tag{3}$$

for j=1,2,...,n. Therefore,

$$D_j = \frac{F_j}{h_j} - \frac{1}{6} Y_j h_j \tag{4a}$$

and

$$C_j = \frac{F_{j+1}}{h_j} - \frac{1}{6} Y_{j+1} h_j \tag{4b}$$

Thus by using equations (4), we can rewrite equation (2) as

$$S_j(s) = \frac{Y_j}{6h_j}(s_{j+1} - s)^3 + \frac{Y_{j+1}}{6h_j}(s - s_j)^3$$

$$+ \left(\frac{F_j}{h_j} - \frac{Y_j h_j}{6}\right)(s_j - s) + \left(\frac{F_{j+1}}{h_j} - \frac{Y_{j+1}\, h_j}{6}\right)(s - s_j) \qquad (5)$$

Finally $S'(s)$ must be continous at the points $s=s_1, s_2, \ldots, s_n$. Therefore, differentiating equation (5) yields

$$S'_j(s) = \frac{-Y_j}{2h_j}(s_{j+1} - s)^2 + \frac{Y_{j+1}}{2h_j}(s - s_j)^2 - \frac{F_j}{h_j} + \frac{Y_j h_j}{6}$$

$$+ \frac{F_{j+1}}{h_j} - \frac{Y_{j+1}\, h_j}{6} \qquad (6)$$

Thus equation (6) gives the slope of the cubic function that represents the approximation of $F(s)$ for

$$s_j \leq s \leq s_{j+1}$$

Since the slope is required to be continous at each interior point:

$$S'_1(s_2) = S'_2(s_2)$$

$$S_2(s_2) = S_3(s_3)$$

$$\vdots$$

$$S_{n-2}(s_{n-1}) = S_{n-1}(s_{n-1})$$

Therefore, using equation (6) and this idea of continuity, we obtain the following equalities:

$$S_j'(s_{j+1}) = -\frac{Y_{j+1}\, h_{j+1}^2}{2h_{j+1}} - \frac{F_{j+1}}{h_{j+1}} + \frac{Y_{j+1}\, h_{j+1}}{6} + \frac{F_{j+2}}{h_{j+1}} - \frac{Y_{j+2}\, h_{j+1}}{6}$$

$$S_j(s_{j+1}) = S_{j+1}(s_{j+1})$$

$$S_{j+1}(s_{j+1}) = -\frac{Y_{j+1}\, h_{j+1}^2}{2h_{j+1}} - \frac{F_{j+1}}{h_{j+1}} + \frac{Y_{j+1}\, h_{j+1}}{6} + \frac{F_{j+2}}{h_{j+1}} - \frac{Y_{j+2}\, h_{j+1}}{6}$$

or $$\frac{h_j}{6} Y_j + \left(\frac{h_j + h_{j+1}}{3}\right) Y_{j+1} + \frac{h_{j+1}}{6} Y_{j+2} = \frac{1}{h_j} F_j - \left(\frac{1}{h_j} + \frac{1}{h_{j+1}}\right) F_{j+1} + \frac{1}{h_{j+1}} F_{j+2}$$

Now, replacing j by j-1 and multiplying by 6 leads to the following equation:

$$h_{j-1}\, Y_{j-1} + 2(h_{j-1} + h_j) Y_j + h_j\, Y_{j+1} = E_j \qquad (7a)$$

where

$$E_j = 6\left[\frac{F_{j-1}}{h_{j-1}} - \left(\frac{1}{h_{j-1}} + \frac{1}{h_j}\right) F_j + \frac{1}{h_j} F_{j+1}\right] \qquad (7b)$$

We note that E_j for $j=2,3,\ldots,n-1$ can be calculated from the known function. By letting $j=2,3,\ldots n-1$, we form a tridiagonol system of equations.

$$
\begin{aligned}
&h_1 Y_1 + m_2 Y_2 + h_2 Y_3 + 0 + 0 + \cdots = E_2 \\
&0 + h_2 Y_2 + m_3 Y_3 + h_3 Y_4 + 0 + \cdots = E_3 \\
&0 + 0 + h_3 Y_3 + m_4 Y_4 + h_4 Y_5 + \cdots = E_4 \\
&\qquad\qquad \vdots \\
&0 + 0 + \cdots + h_{n-2} Y_{n-2} + m_{n-1} Y_{n-1} + h_{n-1} Y_n = E_{n-1}
\end{aligned}
\tag{8}
$$

where $m_j = 2(h_{j-1} + h_j)$.

The solution of this system of equations can be expressed in the form

$$Y_j = A_j + B_j Y_{j+1}$$

or

$$Y_{j-1} = A_{j-1} + B_{j-1} Y_j \tag{9}$$

Now we substitute equation (9) into equation (8) and find that

$$h_{j-1}(A_{j-1} + B_{j-1} Y_j) + m_j Y_j + h_j Y_{j+1} = E_j \tag{10}$$

or

$$(h_{j-1} B_{j-1}) Y_j + h_j Y_{j+1} = E_j - h_{j-1} A_{j-1}$$

Therefore,

$$Y_j = \frac{E_j - h_{j-1} A_{j-1}}{D} - \frac{h_j}{D} Y_{j+1} \tag{11}$$

where $D = h_{j-1}B_{j-1}+m_j$. Comparing equation (11) with equation (9), we obtain

$$A_j = \frac{E_j - h_{j-1} A_{j-1}}{D} \tag{12}$$

$$B_j = - \frac{h_j}{D} \tag{13}$$

for $j=2,3,\ldots n-1$. These two recursion relationships will become extremely important in the following cases.

In the first case, we consider the second derivatives to be specified at the end points. From equation (9)

$$Y_1 = A_1 + B_1 Y_2$$

where Y_1 is known. Therefore, we let

$$B_1 = 0$$

$$A_1 = Y_1 \tag{14}$$

Then using equations (12) and (13), we can compute A_2 and B_2. Next, we can compute A_3 and B_3 and so on. Now recalling that Y_n is known, we can determine Y_{n-1} from the following equation:

$$Y_{n-1} = A_{n-1} + B_{n-1} Y_n$$

Also,

$$Y_{n-2} = A_{n-2} + B_{n-2} Y_{n-1}$$

$$\vdots$$

$$Y_2 = A_2 + B_2 Y_3$$

Therefore, we can calculate all the Y_i values, and using equation (5), we can evaluate S(s) for any point s.

In the second case, we consider the first derivative at each point to be known. Therefore, from equation (6)

$$S_1'(s_1) = \frac{-Y_1}{2h_1}(h_1)^2 - \frac{F_1}{h_1} + \frac{Y_1 h_1}{6} + \frac{F_2}{h_1} - \frac{Y_2 h_1}{6} = T_1 \qquad (15)$$

where T_1 is the known end condition. Rearranging this equation, we can determine Y_1 in terms of Y_2.

$$T_1 = (-\frac{h_1}{2} + \frac{h_1}{6})Y_1 + (\frac{F_2 - F_1}{h_1}) - \frac{Y_2 h_1}{6}$$

$$-\frac{h_1 Y_1}{3} = \frac{T_1 h_1 - F_2 - F_1}{h_1} + \frac{h_1}{6} Y_2$$

$$Y_1 = \frac{-3(T_1 h_1 - F_2 + F_1)}{h_1^2} - \frac{1}{2} Y_2 \qquad (16)$$

From equation (9),

$$A_1 = \frac{-3(T_1 h_1 - F_2 + F_1)}{h_1^2} \tag{17a}$$

and

$$B_1 = -\frac{1}{2} \tag{17b}$$

Next, A_j and B_j are computed as before. At $s=s_n$, it follows from equation (6) that

$$S'_{n-1}(s_n) = \frac{1}{2} Y_n h_{n-1} - \frac{F_{n-1}}{h_{n-1}} + \frac{Y_{n-1} h_{n-1}}{6} + \frac{F_n}{h_{n-1}}$$

$$- \frac{Y_n h_{n-1}}{6} = T_2$$

$$\frac{h_{n-1}}{6} Y_{n-1} + \frac{1}{3} h_{n-1} Y_n + \frac{F_n - F_{n-1}}{h_{n-1}} = T_2 \tag{18}$$

From equation (9), it follows that

$$Y_{n-1} = A_{n-1} + B_{n-1} Y_n$$

$$\frac{h_{n-1}}{6} Y_{n-1} = (A_{n-1} + B_{n-1} Y_n) \frac{h_{n-1}}{6} \tag{19}$$

Next, subtracting equation (19) from equation (18) and collecting terms leads to

$$\frac{1}{3} h_{n-1} Y_n + \frac{F_n - F_{n-1}}{h_{n-1}} = T_2 - \frac{h_{n-1}}{6} [A_{n-1} + B_{n-1} Y_n]$$

$$Y_n = \frac{-A_{n-1} h_{n-1}^2 - 6(F_n - F_{n-1}) + 6T_2 h_{n-1}}{(B_{n-1} + 2)h_{n-1}^2} \qquad (20)$$

Now, the values for y_i are computed in the manner we described earlier.

After the Y_j have been calculated, we can find the value of S(s), using equation (5), anywhere in the interval s_1 to s_n.

Appendix C

VMCON

The subroutine VMCON is an optimization scheme developed at Argonne National Laboratory under a contract with the Department of Energy. The subroutine is based on Powell's method for a quadratic programming approximation of a general nonlinear optimization problem. This discussion will exactly parallel the work presented by Crane, Hillstrom, and Minkoff (1980). However, in this appendix, we will describe the method as applied to the constrained sail problem. For a general overview of VMCON, we refer the reader to Crane's work (1980).

As stated above, Powell's method approximates the general nonlinear problem as a quadratic programming problem. In other words, the nonlinear objective function is approximated by a quadratic objective function, and the nonlinear constraint is approximated by a linear constraint function. Unfortunately, the sail problem is characterized by an extremely nonlinear constraint. As a result, the linear approximation is the major source of error in the formulation of the problem, and premature termination of the algorithm is usually due to this large error. Therefore, a significant improvement could result from either a better approxi-

mation of the constraint or a more nearly linear separation criterion.

As the initial step, we write the objective function and its constraints in the form of a Lagrangian function

$$L(x,\lambda)=f(x)-\lambda\epsilon(x)$$

where $f(x)$ is the function to be optimized, $\epsilon(x)$ is the constraint, and λ is a parameter called a Lagrange multiplier. In this case,

$$f(x)=-DRIVE(\theta)$$

$$C(x)=Sep(\theta)$$

Now for x^* to be an optimum solution, there must exist an associated Lagrange multiplier, λ^*, such that

$$\nabla_x(x^*,\lambda^*)=\nabla f(x^*)-\lambda^*\nabla C(x^*)=0$$

$$\lambda^*\geq 0$$

$$\lambda^* C(x^*)=0$$

and

$$C(x^*)\geq 0$$

These conditions are known as the Kuhn-Tucker conditions. The first condition states that for a minimum the gradient of the Lagrangian is zero. For the unconstrained problem, this minimum correspondes to the global minimum of $f(x)$.

To present an overview of Powell's method, we first approximate the general problem by the quadratic programming problem. Next, we solve the quadratic problem to determine

a feasible search direction. At this point, we test for convergence of the solution. If the solution is not within a specified tolerance, we then do a one-dimensional minimization in this direction. This proceedure is then repeated until the solution converges or the solution diverges and the algorithm prematurely terminates. A flow chart of this algorithm is presented in figure 27.

As a first step in the j-th iteration, we approximate the Lagrangian problem and the constraints as

$$\text{Min } Q(\delta)=f(x^{j-1})+\delta^T\nabla f(x^{j-1})+.5\delta^T B(x^{j-1},\lambda^{j-1})\delta$$

subject to

$$\nabla C(x^{j-1})\delta^j+C(x^{j-1})\geq 0$$

where

$$\delta^j=x-x^j.$$

This δ^j is the feasible search direction for the one dimensional minimization. We then minimize the function

$$\phi(\alpha)=f(x)$$

where

$$x=x^{j-1}+\alpha\delta^j.$$

Next, we follow an iterative proceedure to determine an approximate minimum of ϕ and subsequently x^j. Since δ is a feasible direction, we know x^j is a feasible solution. This x^j is then the solution estimate for the next iteration, and λ^{j-1} is the initial estimate of the Lagrange multiplier.

At this point, we now construct a new estimate of the B matrix. First, we let

$$\xi = x^j - x^{j-1}$$

$$\gamma^* = \nabla_x L(x^j, \lambda^j) - \nabla_x L(x^{j-1}, \lambda^j)$$

$$\theta = \begin{cases} 1 & \xi^T\gamma \geq 0.2\xi^T B\xi \\ \dfrac{0.8\xi^T B\xi}{\xi^T B\xi - \xi^T\gamma} & \xi^T\gamma < 0.2\xi^T B\xi \end{cases}$$

and

$$\gamma = \theta\gamma^* + (1-\theta)B\xi$$

Then,

$$B_{NEW} + B - \frac{B\xi\xi^T B}{\xi^T B\xi} + \frac{\gamma\gamma^T}{\xi^T\xi}$$

This B_{NEW} is then used in the subsequent iteration for x^j.

As indicated in figure 27, a convergence test is made after every solution of the quadratic programming problem. The algorithm terminates if

$$\nabla f(x^{j-1})^T \cdot \delta^j + \lambda^j C(x^{j-1}) < \varepsilon.$$

where ε is an inputed tolerance. Therefore, x^{j-1} is the set of angles which produce the optimum drive without separation. If this inequality is not satisfied, another iteration is performed.

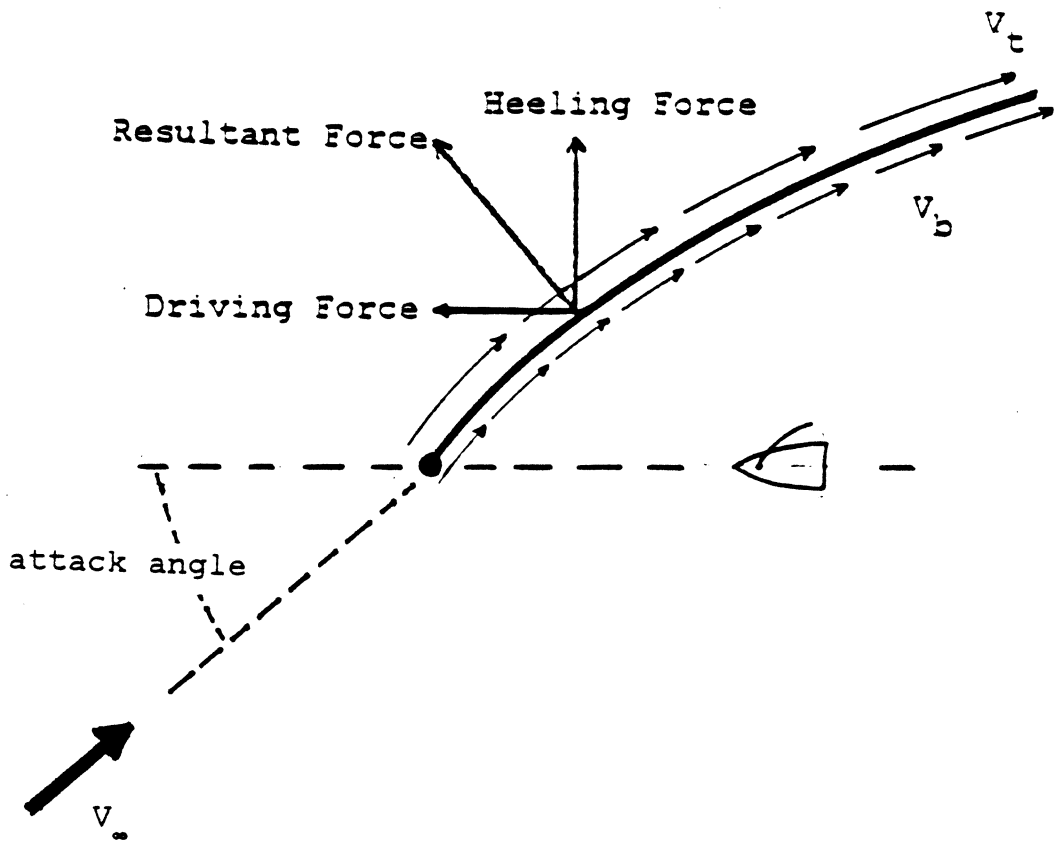

Figure 1: The forces on the sail.

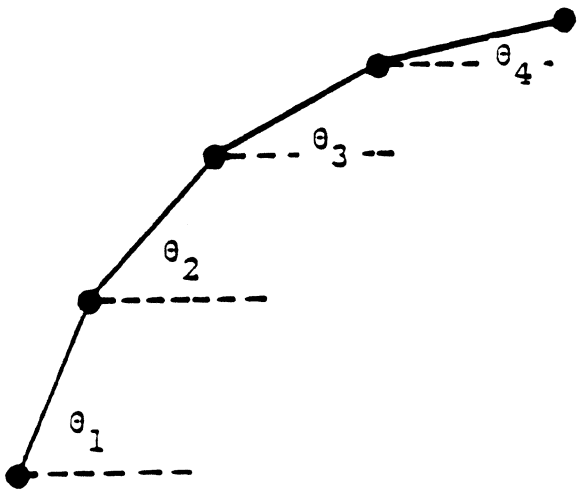

Figure 2: An approximated arc.

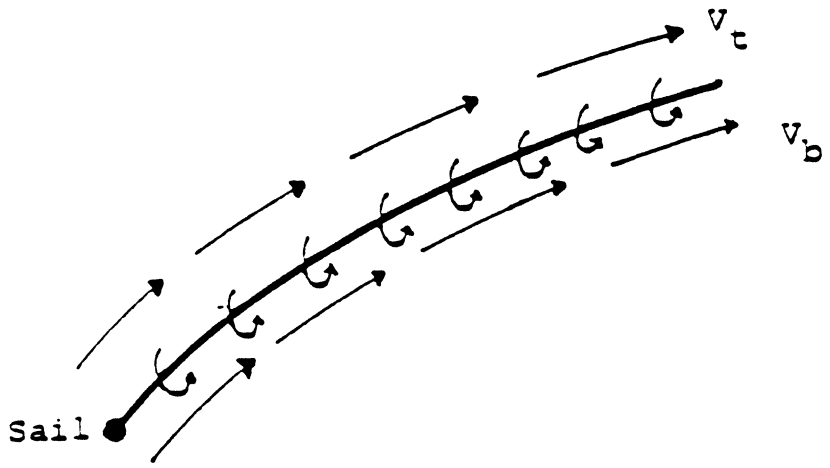

Figure 3: The vortex sheet.

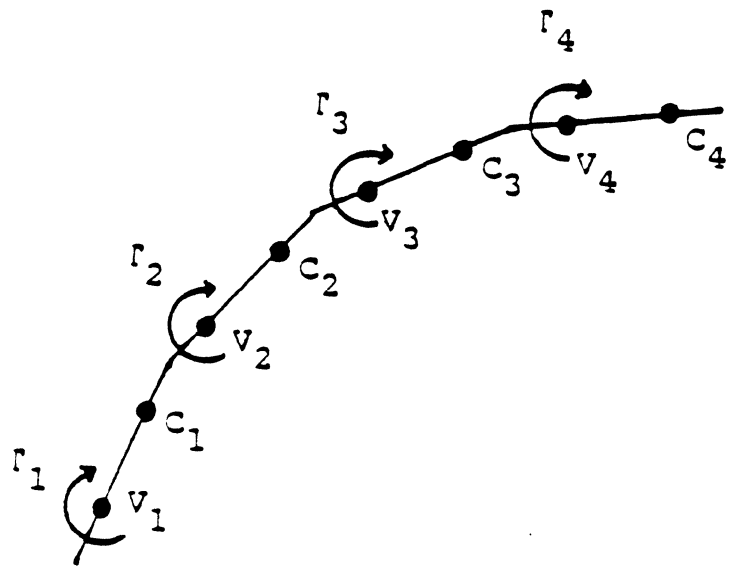

Figure 4: The approximated arc showing the location of the vortex points and the control points.

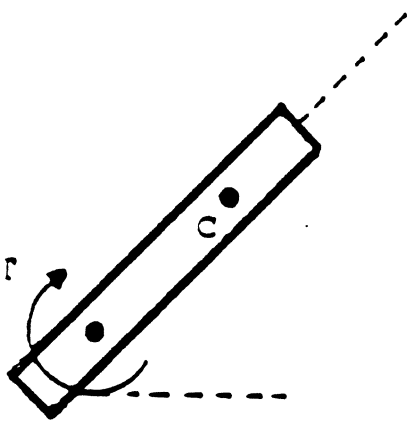

Figure 5: The circulation on a typical surface element.

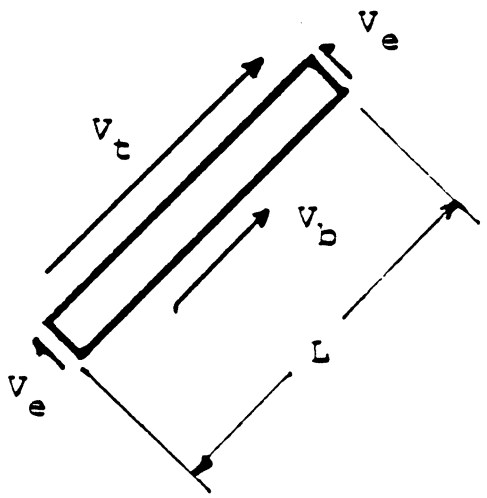

Figure 6: The velocities on a surface element.

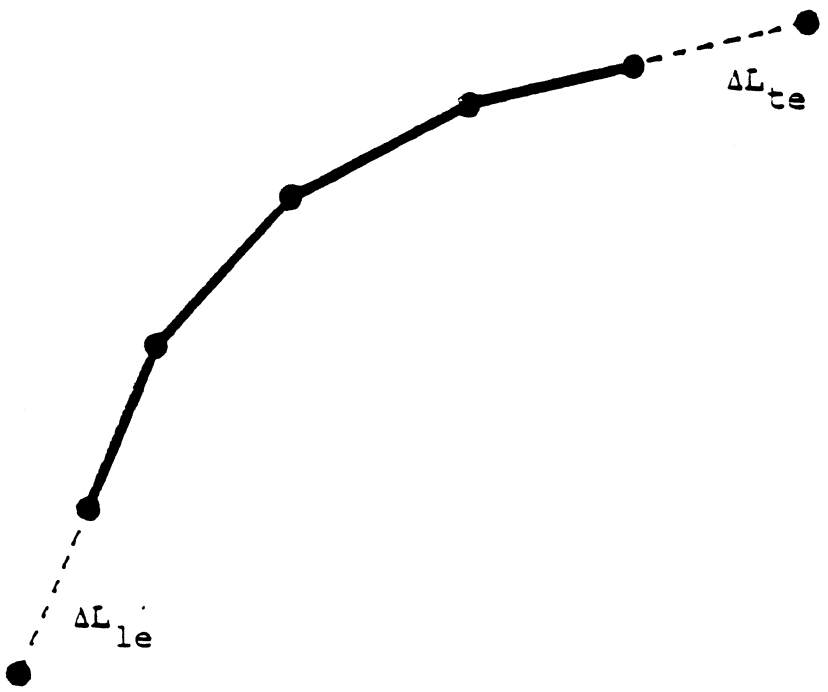

Figure 7: ΔL_{le} and ΔL_{te} represented on a four element model.

Number of Elements	Circulation Calculated	Circulation Exact	Percent Error
9	-3.240	-3.516	7.8
19	-3.385	-3.516	3.7
49	-3.466	-3.516	1.4
99	-3.491	-3.516	.7

Figure 8: Comparison between the closed-form solution and the analytic solution for a 45° circular arc.

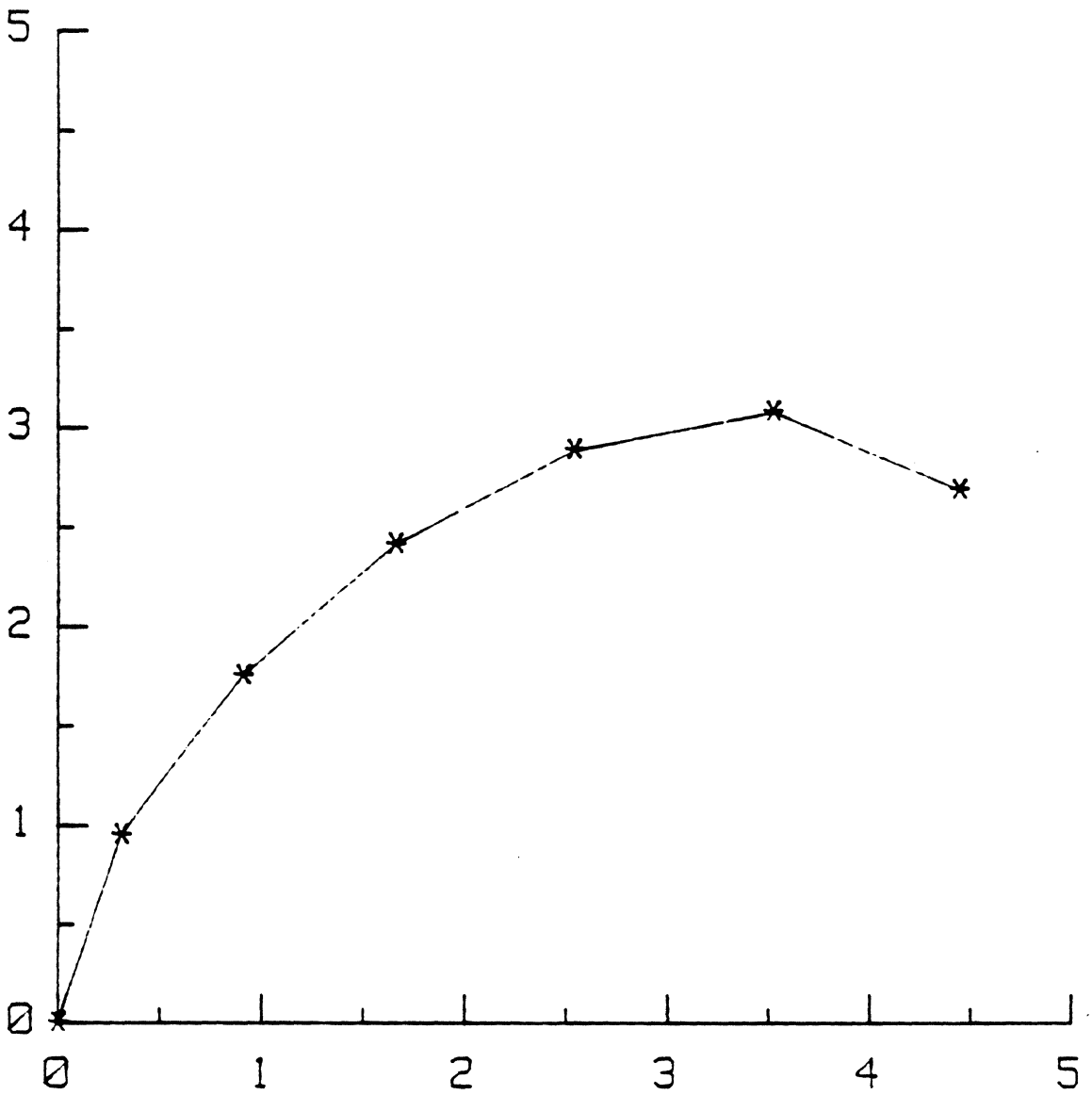

Theta(1)= 71.946
Theta(2)= 53.200
Theta(3)= 41.460
Theta(4)= 28.466
Theta(5)= 11.082
Theta(6)=-23.121

circ=1.274

Figure 9: Unconstrained six-element model at 60° angle of attack.

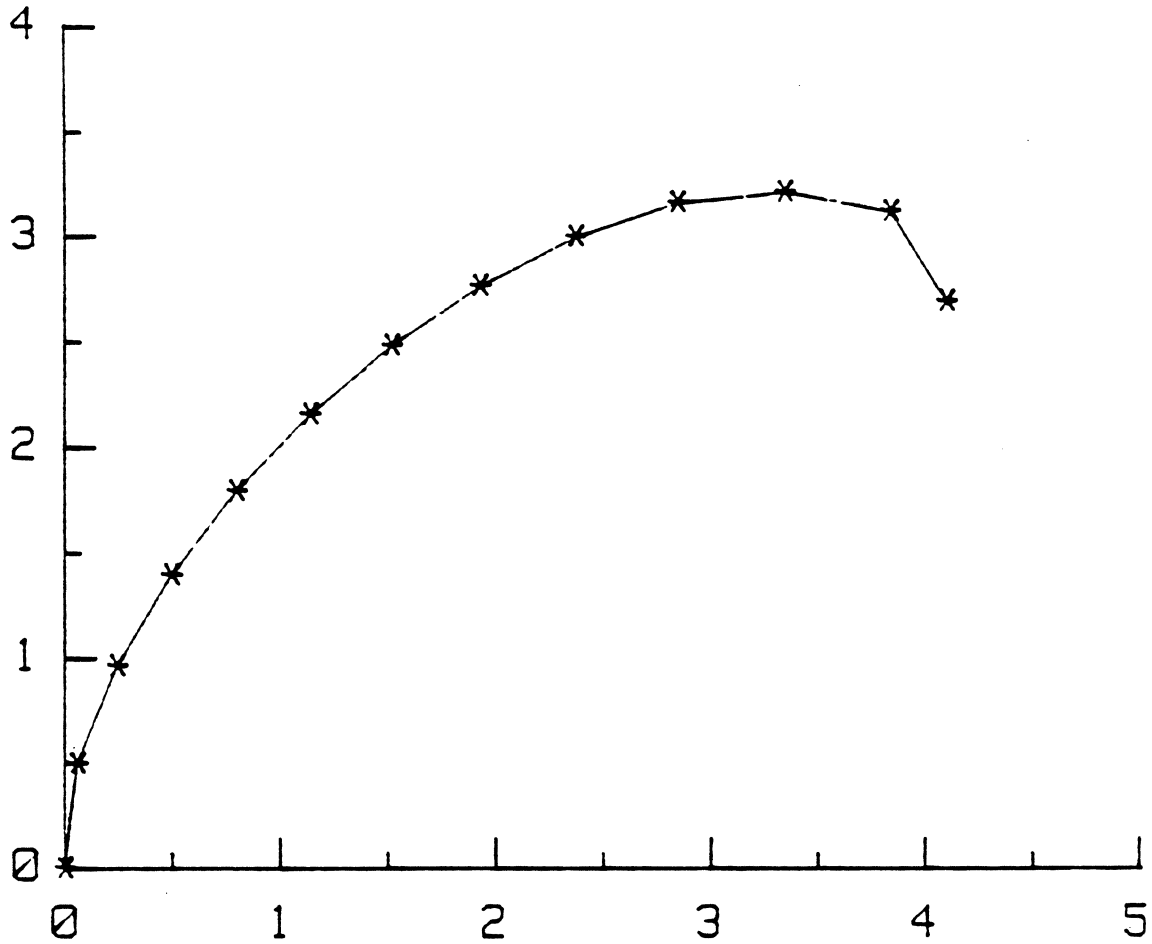

Theta(1)= 83.247
Theta(2)= 68.501
Theta(3)= 59.643
Theta(4)= 52.850
Theta(5)= 46.748
Theta(6)= 40.746
Theta(7)= 34.448
Theta(8)= 27.510
Theta(9)= 18.590
Theta(10)= 5.638
Theta(11)=-10.421
Theta(12)=-58.299

circ=1.429

Figure 10: Unconstrained twelve-element model at 60° angle of attack.

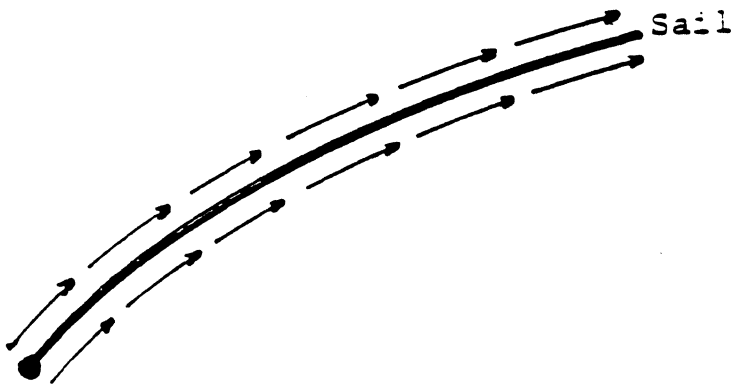

Figure 11: Smooth flow.

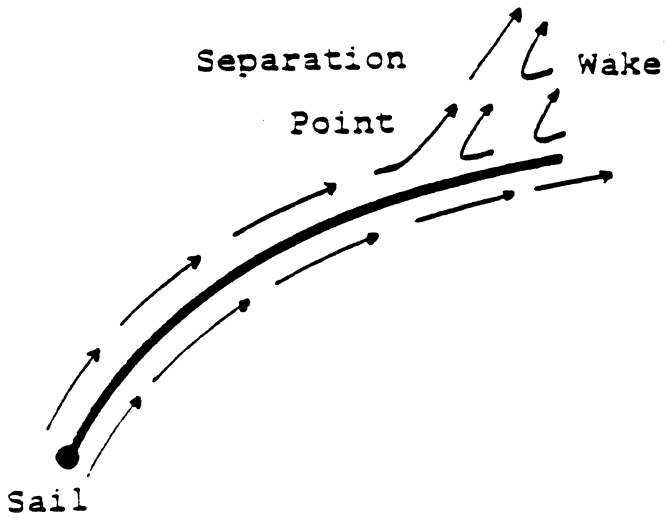

Figure 12: Separated flow.

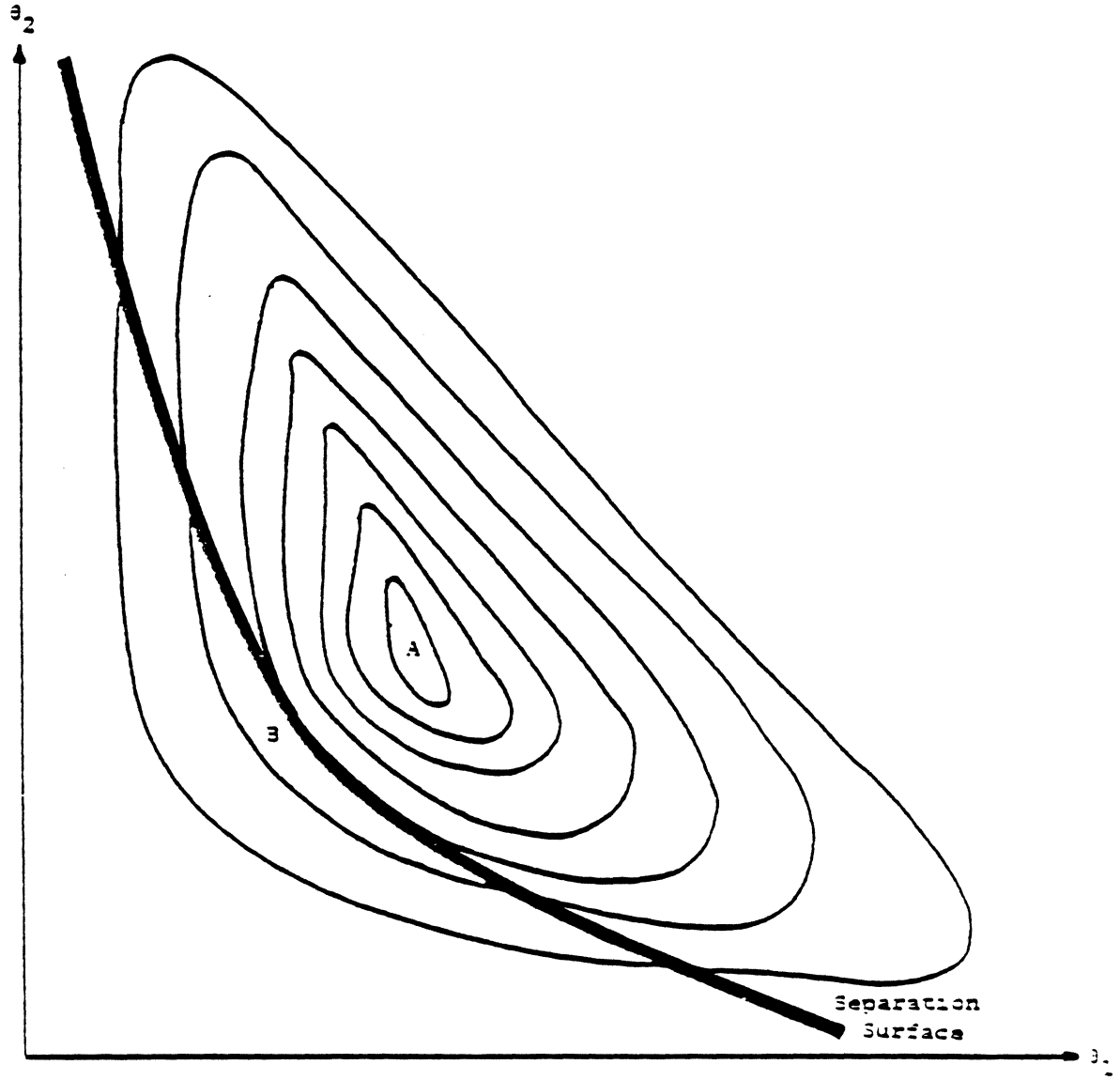

Figure 13: Theoretical and actual extremum.

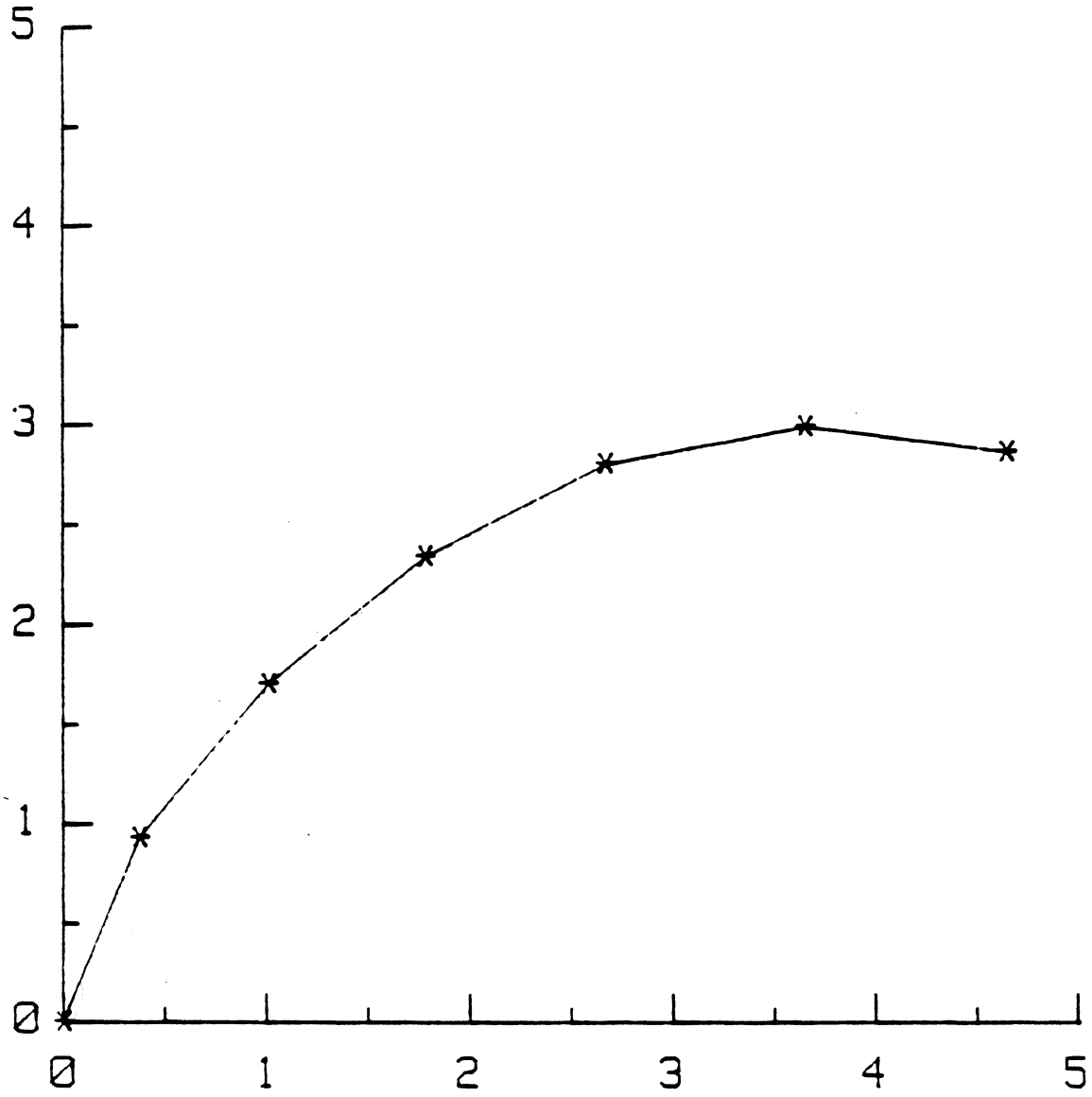

Theta(1)=67.955
Theta(2)=50.752
Theta(3)=39.596
Theta(4)=27.600
Theta(5)=10.814
Theta(6)=-7.445

circ=1.255

Figure 14: Six-element model at 60° angle of attack.

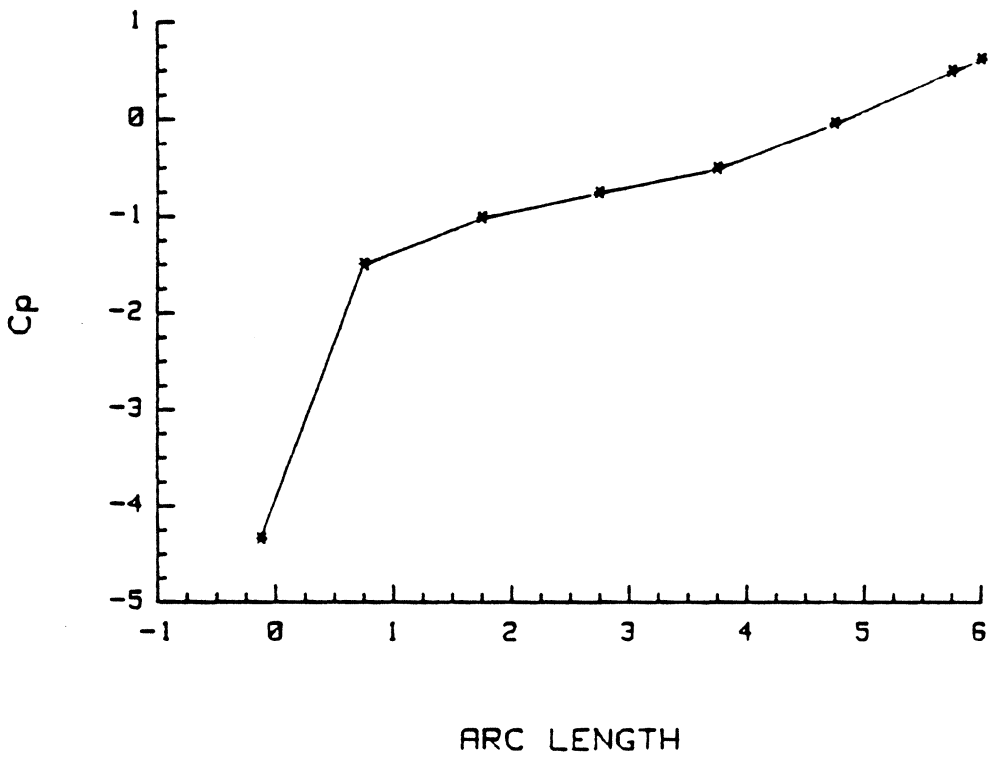

Figure 15: Pressure disturbution over the top of the sail.

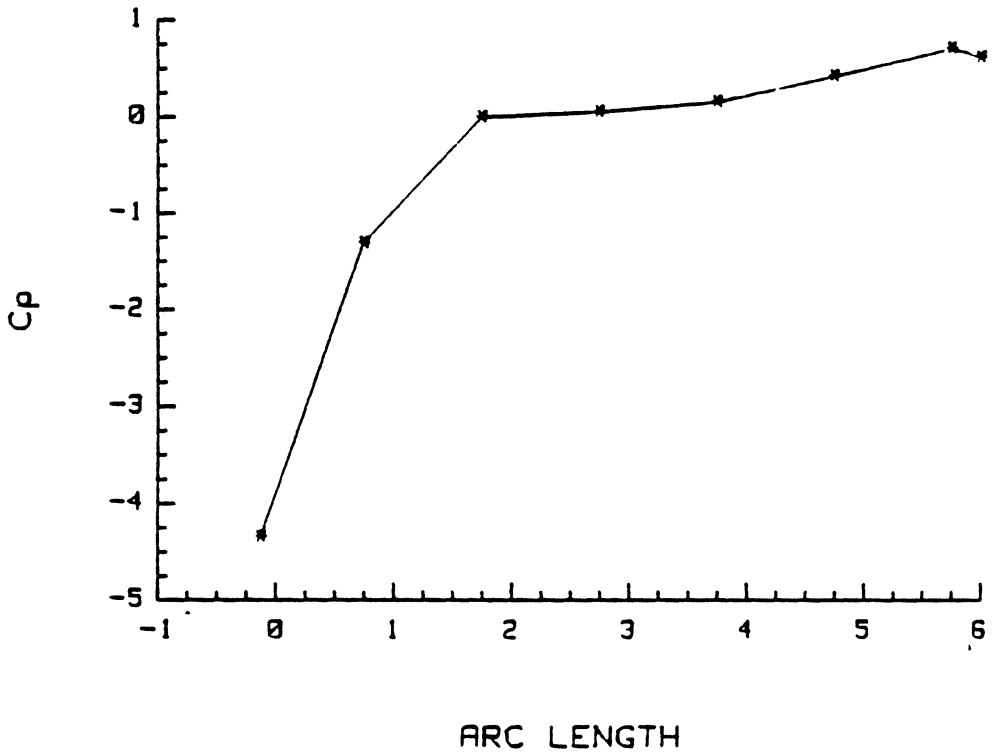

Figure 16: Pressure disturbution over the bottom of the sail.

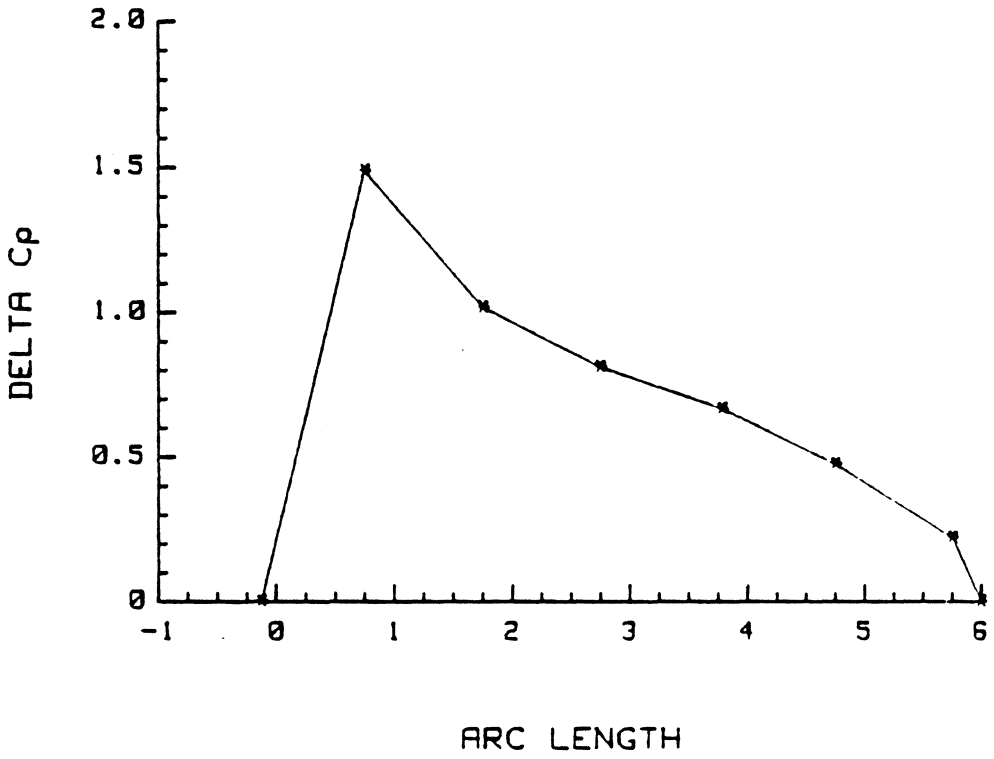

Figure 17: Pressure differential on the sail.

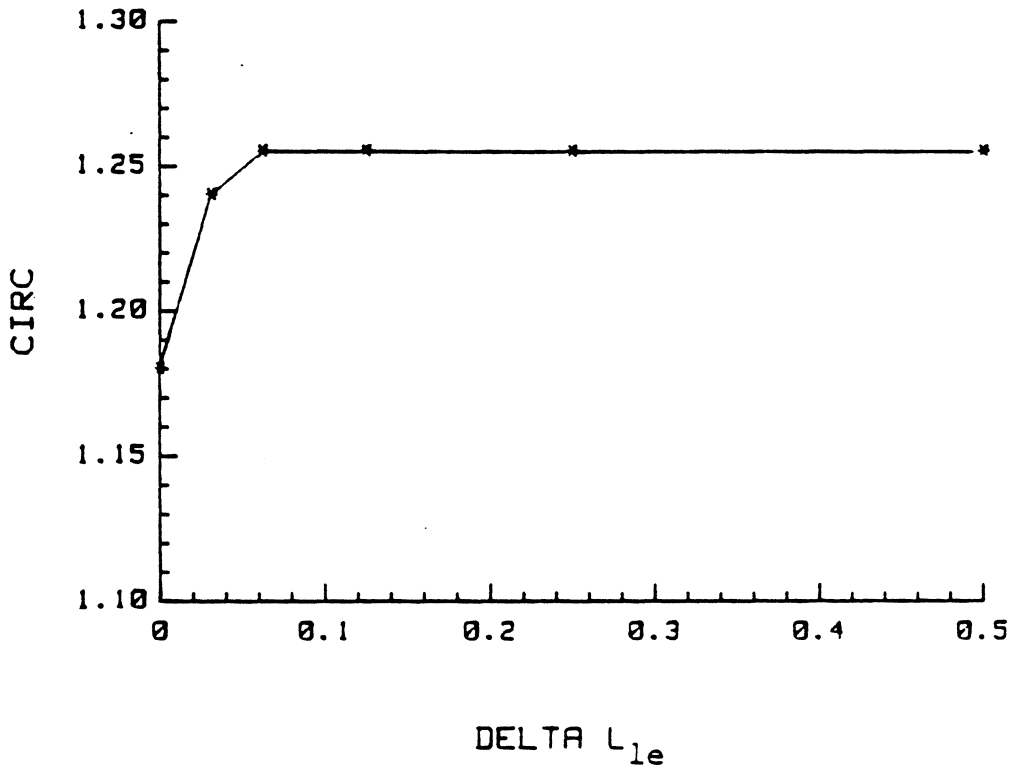

Figure 18: The effect of ΔL_{le} on Circ.

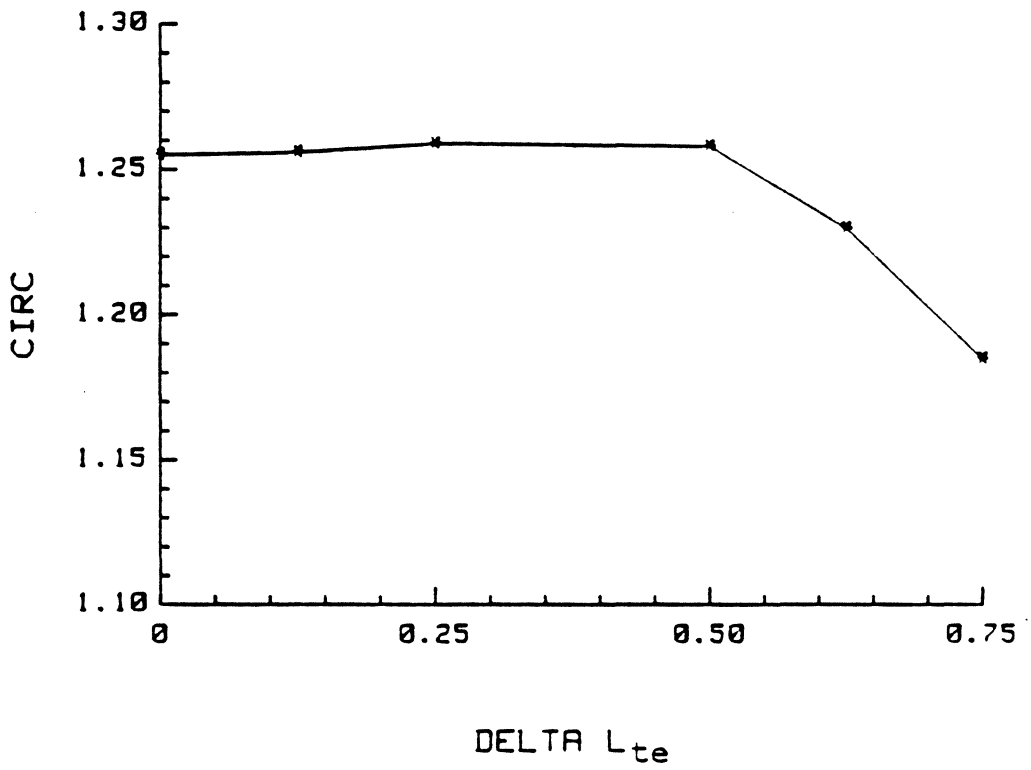

Figure 19: The effect of ΔL_{te} on Circ.

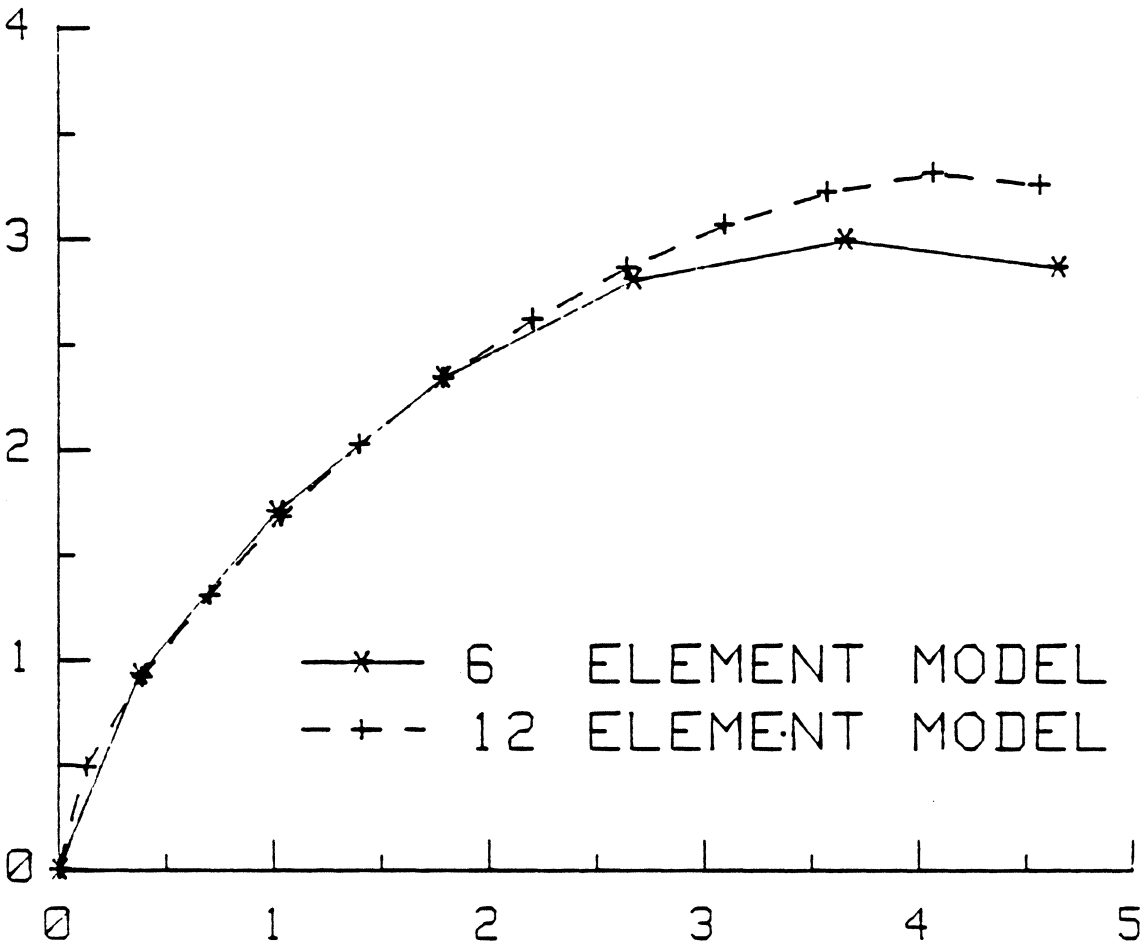

Theta(1)=67.955
Theta(2)=50.752
Theta(3)=39.596
Theta(4)=27.600
Theta(5)=10.814
Theta(6)=-7.445

circ=1.255

Theta(1)= 75.862
Theta(2)= 58.627
Theta(3)= 51.023
Theta(4)= 48.565
Theta(5)= 43.505
Theta(6)= 38.952
Theta(7)= 34.151
Theta(8)= 29.204
Theta(9)= 23.926
Theta(10)= 18.016
Theta(11)= 10.471
Theta(12)= -6.542

circ=1.303

Figure 20: Comparison between a six-element and a twelve-element model at 60° angle of attack.

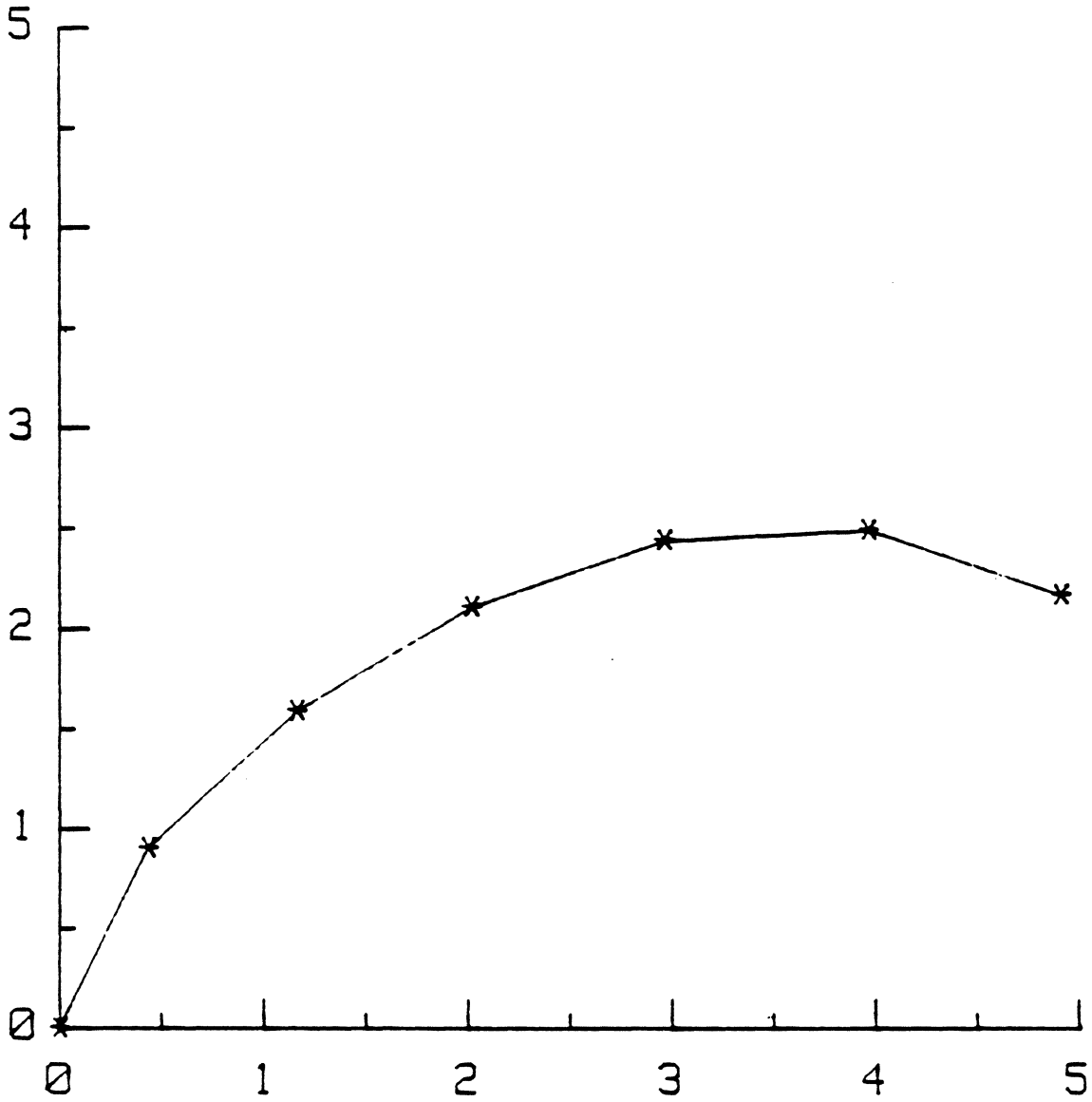

Theta(1)= 64.273
Theta(2)= 43.302
Theta(3)= 31.312
Theta(4)= 19.284
Theta(5)= 2.894
Theta(6)=-18.812

circ=0.865

Figure 21: A six-element model at 45° angle of attack.

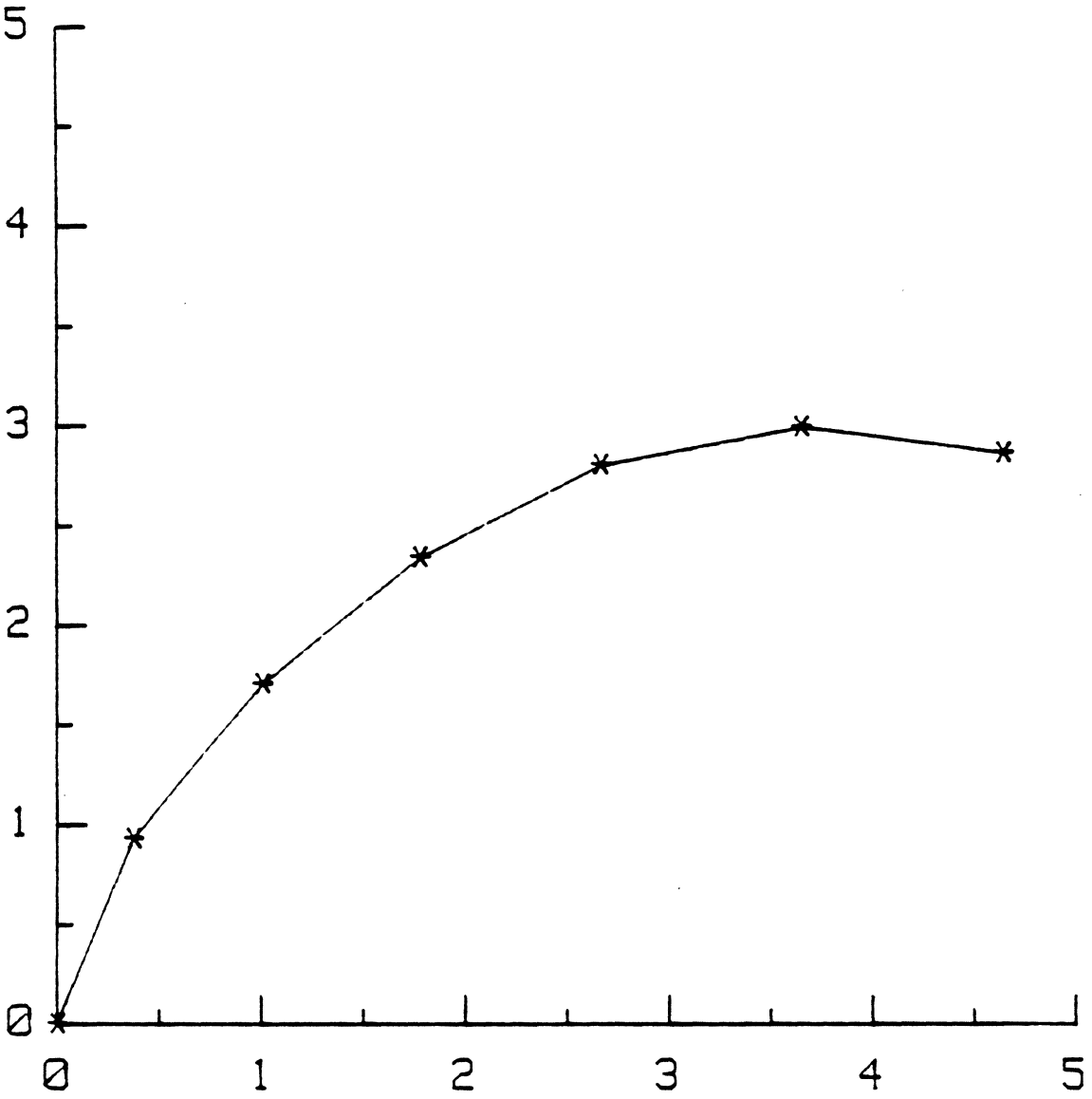

Theta(1)=67.955
Theta(2)=50.752
Theta(3)=39.596
Theta(4)=27.600
Theta(5)=10.814
Theta(6)=-7.445

circ=1.255

Figure 22: A six-element model at 60° angle of attack.

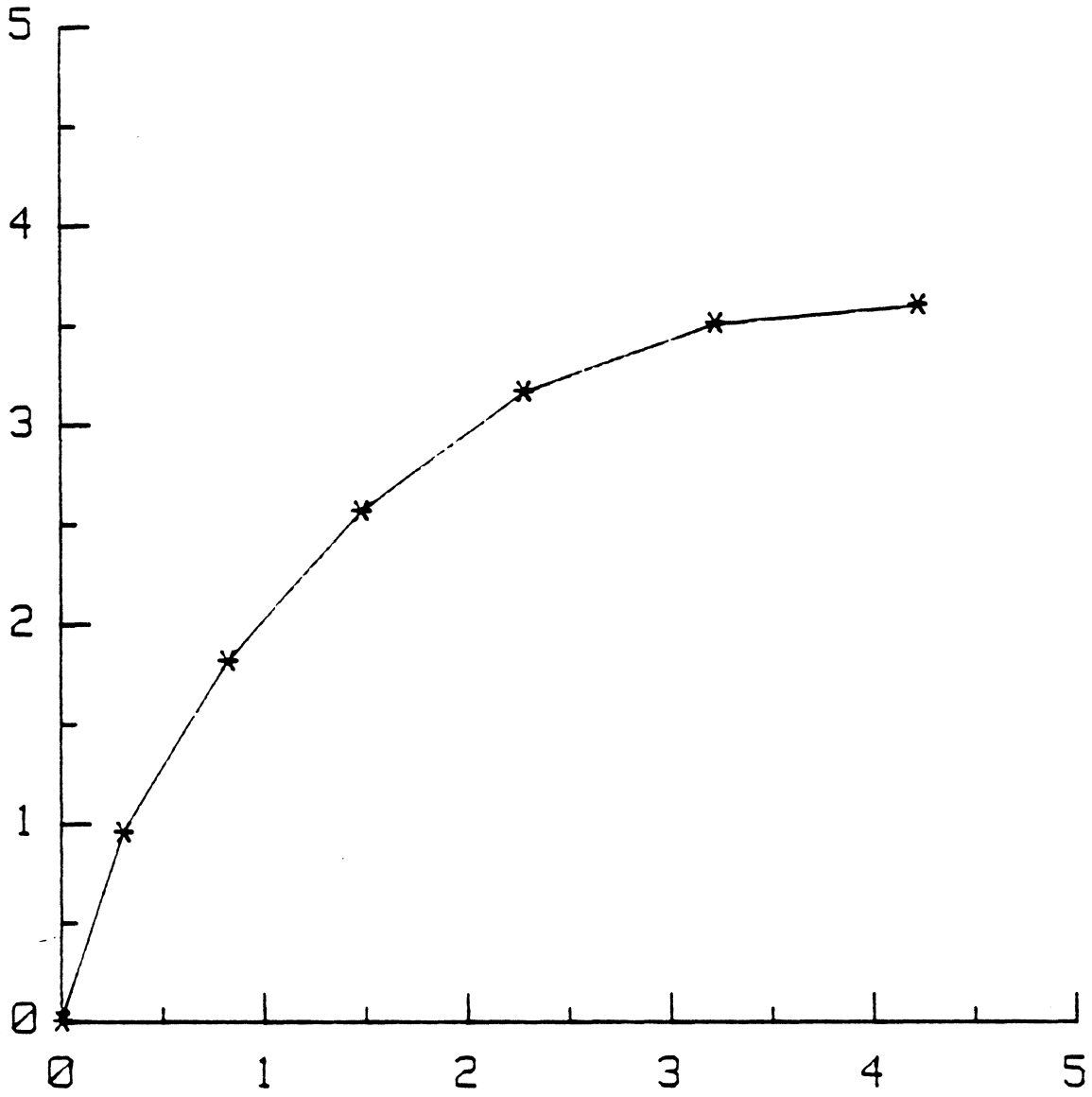

Theta(1)= 72.283
Theta(2)= 59.181
Theta(3)= 48.831
Theta(4)= 36.923
Theta(5)= 19.853
Theta(6)= 5.288

circ=1.628

Figure 23: A six-element model at 75° angle of attack.

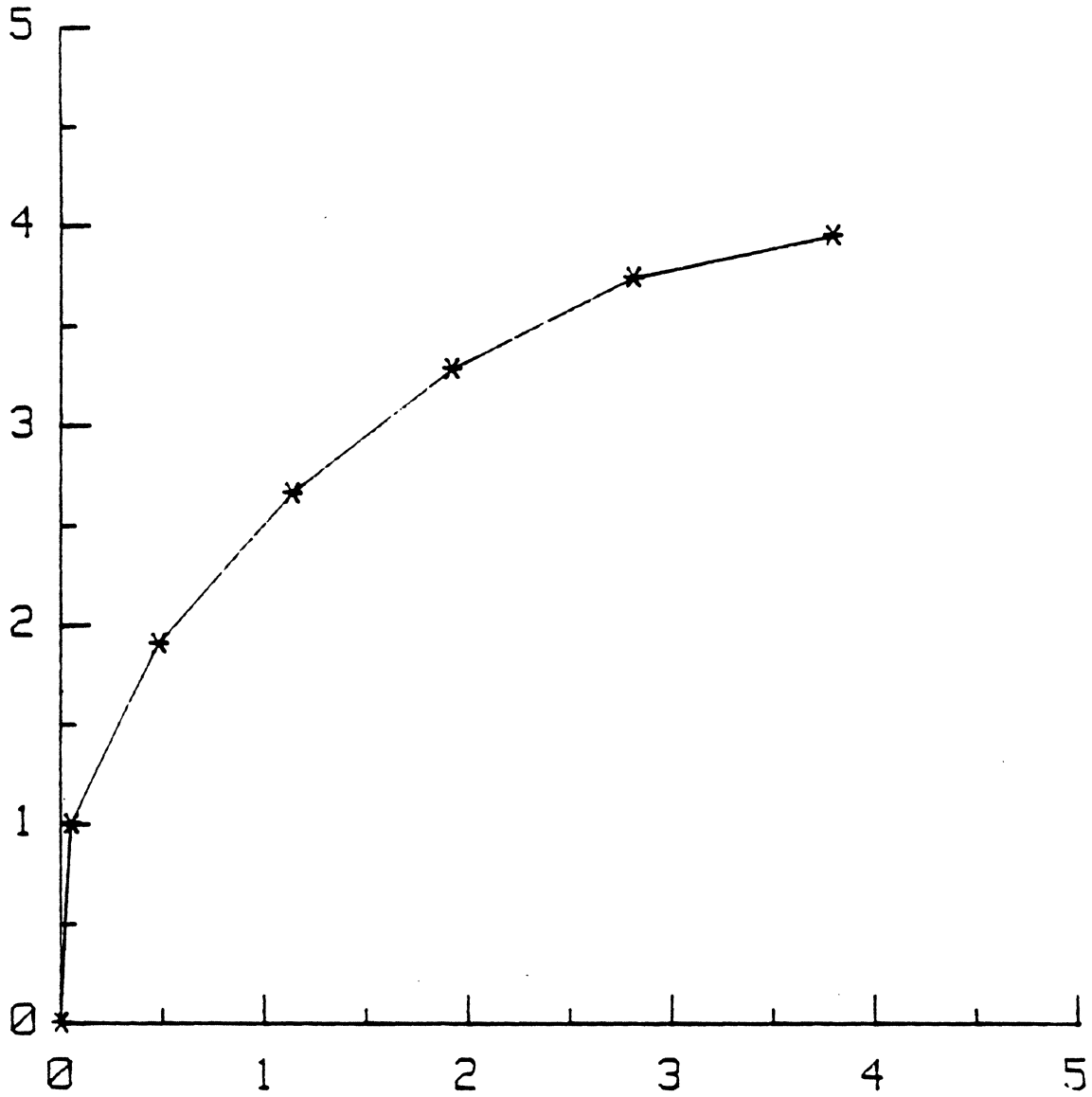

Theta(1)= 87.120
Theta(2)= 64.596
Theta(3)= 49.198
Theta(4)= 38.450
Theta(5)= 26.972
Theta(6)= 12.123

circ=1.975

Figure 24: A six-element model at 90° angle of attack.

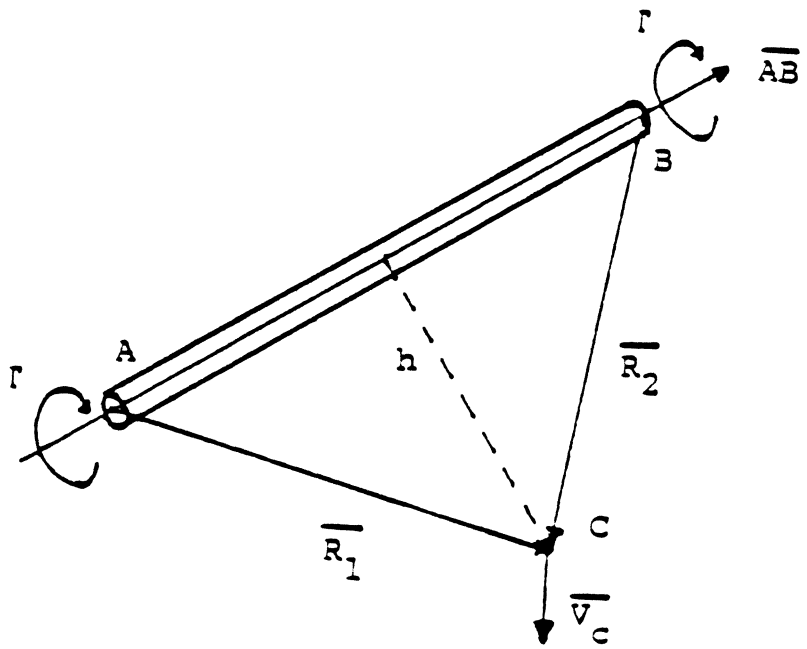

Figure 25: The Biot-Savart law.

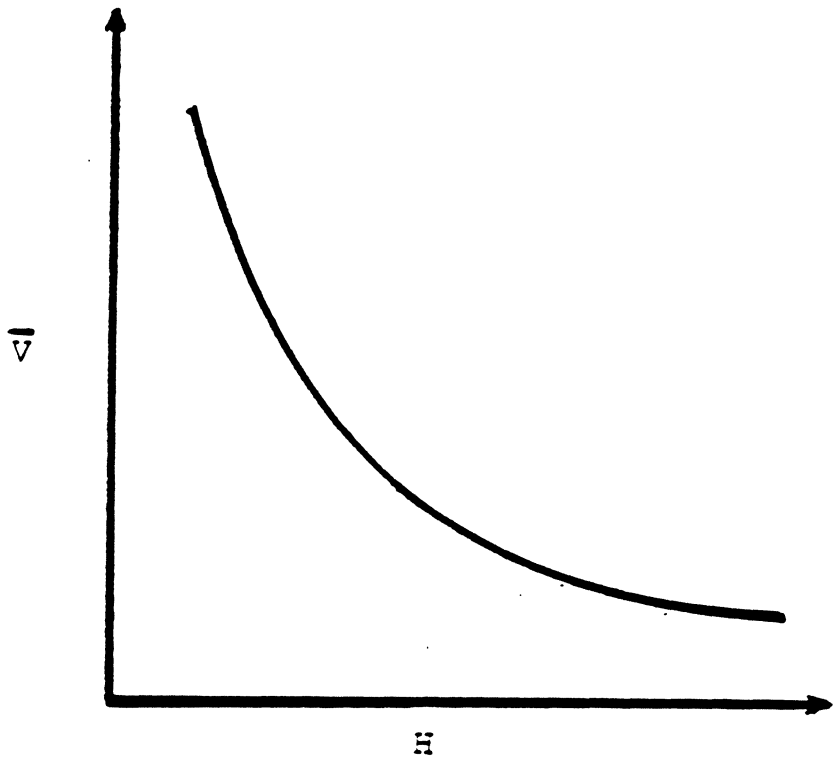

Figure 26: The influence of the circulation as a function of h.

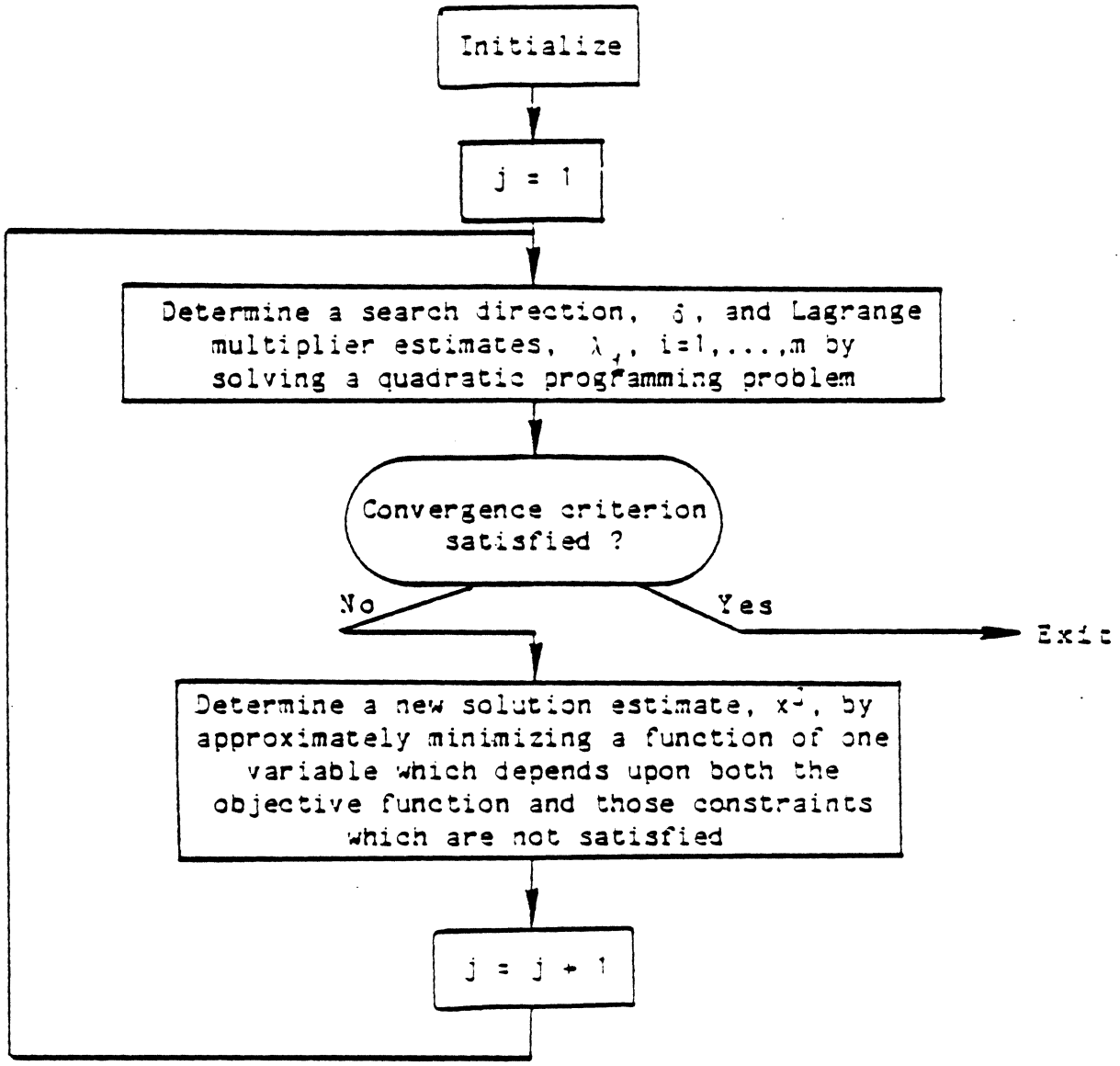

Figure 27: A flow chart of the optimization algorithm used in VMCON

REFERENCES

Cebci, Mosinskis, and Smith. "Calculation of Separation Points in Incompressible Turbulent Flows." Journal of Aircraft Mechanics. Vol. 9 (September, 1972), 618-24.

Crane, Hillstrom, and Minkiff. Solution of the General Non-linear Programming Problem with Subroutine VMCON. (July, 1980) ANL-80-64. Argonne National Laboratory, Argonne Illinois.

Fletcher and Reeves. "Function Minimization by Conjugate Gradients." Computer Journal. Vol. 7 (July, 1964), 149.

Milgram, J. A. "Sailing vessels and Sails." Annual Review of Fluid Mechanics. Vol. 4 (1972), 397.

Stratford, B. S. "The Prediction of Separation of the Turbulent Boundary Layer." Journal of Fluid Mechanics. Vol. 5 (May, 1959), 1-16.

Thrasher, Mook and Nayfeh. "A Computer-Based Method for Analyzing the Flow Over Sails." Proceedings of the fourth Cheasapeake Sailing Yacht Symposium. (January 1979), 119-20.

The vita has been removed from the scanned document

OPTIMIZATION OF SAIL DESIGN

by

Thomas John Dunyak

(ABSTRACT)

This paper is a report on a project to develop a computer-based technique to optimize two dimensional sail design. Overall, we consider two distinct problems. The first problem deals with an unconstrained optimization of the lift. Then, to develop the second problem, we introduce an integrated form of Stratford's separation criterion as a limiting constraint. Throughout the work, we incorporate a vortex lattice analysis to determine the lift on the sail, and in each case, we use an optimization algorithm called VMCON. In the final chapters, we present the results for a series of test cases and describe the areas of future research and development.